THERMAL RADIATION AND CHEMICAL REACTION EFFECTS ON FREE CONVECTIVE HEAT AND MASS TRANSFER FLOW THROUGH AN IRREGULAR CHANNEL

Supported by tetfund TERTIARY EDUCATION TRUST FUND

J. A. Gbadeyan[1], T. L. Oyekunle[2] and J. U. Abubakar[1]
[1]Department of Mathematics, University of Ilorin, Ilorin, Kwara State, Nigeria
[2]Department of Mathematics, College of Education, Oro, Kwara State, Nigeria
*Corresponding author: j.agbadeyan@yahoo.com

Received: January 20, 2017 **Accepted:** March 12, 2017

Abstract: An analysis of the effects of thermal-radiation and chemical reaction on free convective heat and mass transfer flow through an irregular (wavy) vertical channel (made up of a finitely long wavy wall at one end and a parallel flat wall at the other) with constant volumetric heat absorption/generation is carried out. The Rosseland approximation is used to describe radiative heat transfer in the limit of optically thick fluids. The non-dimensional governing equations which comprises of continuity, momentum, energy and species equations were simplified using perturbation method and hence written in terms of zeroth and first order set of coupled differential equations. The solutions of these sets of coupled differential equations were obtained for velocity, temperature, concentration and pressure drop of the fluid, using Adomian decomposition method. The expressions for the fluid variables and those of some characteristics of heat and mass transfer namely Skin friction, Nusselt number and Sherwood number obtained from fluid variables are evaluated numerically and presented graphically for various parameters involved in the problem. By carrying out comparisons with the available data in the literature, our numerical results were validated and excellent agreements were obtained. It is noticed among others, that an increase in the radiation and chemical reaction parameters leads to a decrease in the fluid velocity across the entire width of the channel. The temperature decreases with an increase in the radiation parameter, while an increase in the temperature is observed with an increase in the chemical reaction parameter.

Keywords: Chemical reaction, heat, irregular channel, mass transfer, radiation

Introduction

Radiation is a process in which electromagnetic waves travel through a vacuum. Its effect on fluid flow and heat transfer is important especially in engineering where many processes occur at high temperature, such as the design of pertinent equipment, Nuclear power plants, gas turbines and the various propulsion devices for air craft, missiles, satellites and space vehicles (Srihari and Avinash, 2014).Chemical reaction is a process that leads to transformation of one set of chemical substances to another. The chemical reactions are central to chemical engineering where they are used for synthesis of new compound from natural raw materials such as petroleum, mineral ores and thermite reaction to generate light and heat in pyrotechnics and welding.

Heat transfer is a process by which internal energy from one substance transfers to another while mass transfer is the transport of a substance (mass) in liquid or gaseous media. There are many physical processes in which buoyancy forces resulting from combined thermal and species diffusion play an important role in the convective heat and mass transfer. The engineering applications include the chemical distillatory process, formation and dispersion of fog, design of heat ex-changers, channel type solar energy collectors, and thermo protection system (Rajasekhar *et al.*, 2013). Therefore, it is of great significant interest to look in to the combined effects of heat and mass transfer with radiation and chemical reaction on the fluid flow, because of their applications in many processes occurring both in nature and industries.

In view of these applications, Gbadeyan and Dada (2013) examined the influence of radiation and heat transfer on an unsteady MHD non-Newtonian flow with slip in porous medium. They observed that the temperature increases with a decrease in either the Prandtl number or radiation parameter and also noticed that the velocity profiles decrease as the radiation parameter N or Grashof number decreases. Hayat *et al*. (2010) studied the effect of radiation and magnetic field on the mixed convection stagnation-point flow over a vertical stretching sheet in a porous medium. Shateyi *et al.* (2010) investigated the effects of thermal radiation, Hall currents, Soret and Dufour on MHD flow by mixed convection over a vertical surface in porous media.

In addition, Olanrewaju and Gbadeyan (2011) examined a mathematical model in order to study the effect of Soret, Dufour, chemical reaction, thermal radiation and volumetric heat generation/ absorption on mixed convection stagnation-point flow on an isothermal vertical plate in a porous media. Rajasekhar *et al.* (2013) investigated the effects of chemical reaction, Hall currents on an unsteady mixed convective heat and mass transfer flow of a viscous, electrically conducting fluid in a vertical channel under the influence of an inclined magnetic fluid with heat source. Sudershan *et al*. (2012), studied the effects of the chemical reaction and radiation on free convective MHD flow through a porous medium bounded by vertical surface.

Srihari and Avinash (2014) presented the effect of radiation on an unsteady free convection flow of a viscous incompressible, electrically conducting fluid past an infinite hot vertical porous plate embedded in a porous medium. Olanrewaju *et al.* (2013) analyzed the effect of chemical reaction, thermal radiation, thermal-diffusion and diffusion thermo on hydro-magnetic free convection with heat and mass transfer past a vertical plate with suction/injection. Gbadeyan *et al*. (2011) studied the boundary layer flow induced in a Nano fluid due to a linear stretching sheet in the presence of thermal radiation and induced magnetic field. Loganathan *et al.* (2011) studied the effect of chemical reaction on an unsteady two dimensional laminar flow of a viscous incompressible fluid flow past a semi-infinite vertical plate with variable viscosity and thermal conductivity. They noted that the results pertaining to variable fluid properties differ significantly from those of the constant fluid properties.

The above studies are for flow which is either through a regular channel or over a flat surface. However, it is well known in practice that some degree of wall irregularity usually occurs. Furthermore, the studies of viscous fluid flow and heat transfer over an irregular wall in both horizontal and

vertical passages is receiving considerable attentions in the recent years for its potential applications to physical problems such as transpiration, cooling of re-entry vehicles and rocket boosters, cross-hatching on ablative surfaces and film vaporization in combustion chambers (Vajravelu and Sastri, 1978). Other vital applications in engineering devices and processes include heat ex-changers for viscous liquids in a chemical process and food industry, nuclear reactors, glass manufacturing, crude oil refinement, paper production and other related devices abound (Fasogbon, 2006).

Vajravelu and Sastri (1978) analyzed the effect of irregularity (waviness) of one of the walls on the flow and heat transfer characteristics of an incompressible viscous fluid confined between two long vertical walls. Das and Ahamed (1992) discussed the problem of two dimensional free convection MHD flow of a viscous incompressible fluid between a long vertical irregular wall and a parallel flat wall. Fashogbon and Omolehin (2008) examined the radiation effect on natural convection in an irregular channel. Abubakar (2014) studied the effect of the wall slip on a laminar two dimensional free convective flow of fluid confined between an irregular wall and a flat wall. He discovered that an increase in the slip parameter at the wall leads to a decrease in fluid velocity. Fasogbon (2010) discussed analytically, the studies of heat and mass transfer by free convection in a two dimensional irregular channel. Kumar (2011) studied two dimensional heat transfer of a free convective MHD flow with radiation and temperature dependent heat source of a viscous incompressible fluid in a vertical irregular channel. Davika*et al*. (2013) examined the effects of chemical reaction and heat source on two dimensional free convection MHD flow in an irregular channel with porous medium. Oyekunle (2015) analyzed the effects of thermal-diffusion, diffusion-thermo and radiation on chemically reacting magneto-hydrodynamics flow of heat and mass transfer within an irregular channel. Dada and Disu (2015), discussed two dimensional heat transfer of a free convection MHD flow with radiation and temperature dependent heat source of a viscous incompressible fluid in a porous medium within a wavy channel.

In all the above studies, to the best knowledge of the authors, the effects of the combined thermal radiation and chemical reaction on free convective heat and mass transfer flow through a finitely long vertical irregular channel has not been considered. Therefore, the goal of the present work is to investigate the combined effects of thermal radiation and chemical reaction on free convective heat and mass transfer flow through an irregular channel. In other words, this paper extends the work of Vajravelu and Sastri (1978) and Fashogbon (2010) to study the natural convective heat and mass flow through an irregular channel under the influence of radiation and chemical reaction. The importance of this work is that it improves the protection of properties and lives which is crucial in many petro-chemical engineering applications as well as chemical and hydrometallurgical industries; For example, when dealing with reactive fluid flow through an irregular channel (Adesanya, 2004). The non-dimensional coupled boundary value problem governing fluid flow was perturbed taking into consideration a supplementary term in energy equation due to the constant volumetric heat absorption/generation and the resulting zeroth and first order boundary value problem were solved, using Adomian decomposition method with MAPLE software.

Formulation of the problem

The channel considered, is made up of a finitely long irregular (wavy) wall at one end and a flat wall at the other (The case involving irregular walls at both ends can be similarly treated using the analysis presented in this work). The $X^{'}$-axis is taken to be vertically upward and parallel to the flat wall in the direction of buoyancy, while $Y^{'}$-axis is perpendicular to $X^{'}$-axis in such a way that the position of irregular wall is represented by $Y^{'}=\epsilon^{*}\cos kX^{'}$, $|\epsilon^{*}|<1$ and that of the flat wall is represented by $Y^{'}=d$ (Fig. 1). The flow is considered laminar, two dimensional and steady, all fluid properties are also assumed constant except the density in the buoyancy force term, the viscous dissipation and work done by pressure are considered sufficiently small in comparison with both the flow by conduction, wall temperatures and wall concentrations.

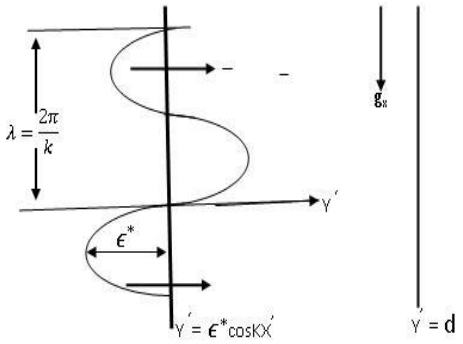

Figure 1: The flow Channel

Based on these assumptions using the usual Boussinesq approximation, the governing equations of steady two dimensional heat and mass transfer are made up of the following continuity, momentum, energy and species equations.

$$\frac{\partial U^{'}}{\partial X^{'}}+\frac{\partial V^{'}}{\partial Y^{'}}=0 \qquad (1)$$

$$\rho(U^{'}\frac{\partial U^{'}}{\partial X^{'}}+V^{'}\frac{\partial U^{'}}{\partial Y^{'}})=-\frac{\partial P^{'}}{\partial X^{'}}+\mu(\frac{\partial^2 U^{'}}{\partial X^{'2}}+\frac{\partial^2 U^{'}}{\partial Y^{'2}})+\rho g_{x\beta_T}(T^{'}-T_s^{'})+\rho g_{x\beta C}(C^{'}-C_s^{'}) \qquad (2)$$

$$\rho(U^{'}\frac{\partial V^{'}}{\partial X^{'}}+V^{'}\frac{\partial V^{'}}{\partial Y^{'}})=-\frac{\partial P^{'}}{\partial Y^{'}}+\mu(\frac{\partial^2 V^{'}}{\partial X^{'2}}+\frac{\partial^2 V^{'}}{\partial Y^{'2}}) \qquad (3)$$

$$\rho C_p(U^{'}\frac{\partial T^{'}}{\partial X^{'}}+V^{'}\frac{\partial T^{'}}{\partial Y^{'}})=k(\frac{\partial^2 T^{'}}{\partial X^{'2}}+\frac{\partial^2 T^{'}}{\partial Y^{'2}})+Q-\frac{\partial q_r}{\partial X^{'}}-\frac{\partial q_r}{\partial Y^{'}} \qquad (4)$$

$$(U^{'}\frac{\partial C^{'}}{\partial X^{'}}+V^{'}\frac{\partial C^{'}}{\partial Y^{'}})=D(\frac{\partial^2 C^{'}}{\partial X^{'2}}+\frac{\partial^2 C^{'}}{\partial Y^{'2}})-k_1(C^{'}-C_s^{'}) \qquad (5)$$

The corresponding boundary conditions of the problem are taken as

$$\left.\begin{aligned} &U^{'}=0, \quad V^{'}=0, \quad T^{'}=T_w^{'} \quad C^{'}=C_w^{'} \quad on \quad Y^{'}=\in^{*}\cos KX^{'} \\ &U^{'}=0, \quad V^{'}=0, \quad T^{'}=T_1^{'} \quad C^{'}=C_1^{'} \quad on \quad Y^{'}=d \end{aligned}\right\} \tag{6}$$

On introducing the non-dimensional variables into equations (1)-(6) we have

$$\frac{\partial u}{\partial x}+\frac{\partial v}{\partial y}=0 \tag{7}$$

$$u\frac{\partial u}{\partial x}+v\frac{\partial u}{\partial y}=-\frac{\partial p}{\partial x}+\frac{\partial^2 u}{\partial x^2}+\frac{\partial^2 u}{\partial y^2}+G1\theta+G2c \tag{8}$$

$$u\frac{\partial v}{\partial x}+v\frac{\partial v}{\partial y}=-\frac{\partial p}{\partial x}+\frac{\partial^2 v}{\partial x^2}+\frac{\partial^2 v}{\partial y^2} \tag{9}$$

$$p_r\left(u\frac{\partial \theta}{\partial x}+v\frac{\partial \theta}{\partial y}\right)=\omega\left(\frac{\partial^2 \theta}{\partial x^2}+\frac{\partial^2 \theta}{\partial y^2}\right)+\alpha \tag{10}$$

$$S_c\left(u\frac{\partial c}{\partial x}+v\frac{\partial c}{\partial y}\right)=\frac{\partial^2 c}{\partial x^2}+\frac{\partial^2 c}{\partial y^2}-gc \tag{11}$$

The corresponding boundary conditions are

$$u=v=0, \theta=c=1 \qquad on \quad y=\in\cos\lambda x \tag{12}$$

$$u=v=0, \theta=m1,\ c=m2 \qquad on \quad y=1 \tag{13}$$

The following non-dimensional variables were used

$$(x,y)=\frac{1}{d}(X^{'},Y^{'}),\ (u.,v)=\frac{d}{\nu}(U^{'},V^{'}),\ \lambda=kd,\ \in=\frac{\in^{*}}{d},\ p_s=\frac{P_s^{'}d^2}{\rho\nu^2},\ \theta=\frac{T^{'}-T^{'}_s}{T_w-T_s},\ p=\frac{P^{'}d^2}{\rho\nu^2}$$

$$T_s\neq T_{w,}\ \ c=\frac{C^{'}-C^{'}_s}{C_w-C_s},\ \ C_s\neq C_w\ ,\ G1=\frac{d^3g\beta_T(T_w-T_s)}{\nu^2},\ \ G2=\frac{d^3g\beta_C(C_w-C_s)}{\nu^2},\ \ p_r=\frac{\mu c_p}{k}, \tag{14}$$

$$N=\frac{4\sigma_\infty T^3{}_\infty}{k_\infty k},\ \ \alpha=\frac{Qd^2}{k(T_w-T_s)},\ \ S_c=\frac{\nu}{D},\ \ \omega=1+\frac{4}{3}N,\ \ g=\frac{k_1d^2}{D},\ \ m1=\frac{T_1-T_s}{T_w-T_1},\ \ m2=\frac{C_1-C_s}{C_w-C_1}$$

From the engineering point of view, the important characteristics of the flow are shearing stress, the rate of heat and mass transfer at the wall. These are defined as follows;

$$S_f=\frac{\partial u}{\partial y}+\frac{\partial v}{\partial x}|_{y=0,1},\ N_u=\frac{\partial\theta}{\partial y}|_{y-0,1}\ and\ S_h=\frac{\partial c}{\partial y}|_{y=0,1} \tag{15}$$

Method of solution

The irregularity of the wall is assumed small, hence, it is appropriate to seek a perturbation solution for small ϵ. The limit ϵ = 0 is, of course, the limit of a smooth flat wall, for which thesolution is well known. Thus we take the flow field variables, velocity, pressure, temperature and concentration as

$$u(x,y)=u_0(y)+\in u_1(x,y),\ v(x,y)=\in v_1(x,y),\ \ p(x,y)=p_0(x)+\in p_1(x,y),\theta(x,y)=$$
$$\theta_0(y)+\in\theta_1(x,y),\ c(x,y)=c_0(y)+\in c_1(x,y) \tag{16}$$

Introducing equations (16) into equations (7)-(13), we obtained the following set of coupled zeroth and first order boundary value problems.

For zeroth-order, we have

$$\frac{d^2u_0}{dy^2} + G1\theta_0 + G2c_0 = C \tag{17}$$

$$\frac{d^2\theta_0}{dy^2} = -\frac{\alpha}{\omega} \tag{18}$$

$$\frac{d^2c_0}{dy^2} - gc_0 = 0 \tag{19}$$

with the following boundary conditions

$$\left.\begin{aligned} u_0 = 0,\ \theta_0 = c_0 = 1 \quad on \quad y = 0 \\ u_0 = 0,\ \theta_0 = m1, c_0 = m2 \ on \ \ y = 1 \end{aligned}\right\} \tag{20}$$

Where $C = \frac{\partial p_0}{\partial x}$, and without loss of generality is taken to be zero(Vajravelu and Sastri, 1978; Fasogbon, 2010).

On the other hand, the set of first order boundary value problem is

$$\frac{\partial u_1}{\partial x} + \frac{\partial v_1}{\partial y} = 0 \tag{21}$$

$$u_0\frac{\partial u_1}{\partial x} + v_1\frac{\partial u_0}{\partial y} = -\frac{\partial p_1}{\partial x} + \frac{\partial^2 u_1}{\partial x^2} + \frac{\partial^2 u_1}{\partial y^2} + G1\theta_1 + G2c_1 \tag{22}$$

$$u_0\frac{\partial v_1}{\partial x} = -\frac{\partial p_1}{\partial y} + \frac{\partial^2 v_1}{\partial x^2} + \frac{\partial^2 v_1}{\partial y^2} \tag{23}$$

$$p_r\left(u_0\frac{\partial \theta_1}{\partial x} + v_1\frac{\partial \theta_0}{\partial y}\right) = \omega\left(\frac{\partial^2\theta_1}{\partial x^2} + \frac{\partial^2\theta_1}{\partial y^2}\right) \tag{24}$$

$$S_c\left(u_0\frac{\partial c_1}{\partial x} + v_1\frac{\partial c_0}{\partial y}\right) = \frac{\partial^2 c_1}{\partial x^2} + \frac{\partial^2 c_1}{\partial y^2} - gc_1 \tag{25}$$

With the boundary conditions

$$\left.\begin{aligned} u_1 = -u_0',\quad v_1 = 0, \theta_1 = -\theta_0', c_1 = -c_0' \quad on \quad y = 0 \\ u_1 = 0, \quad v_1 = 0, \quad \theta_1 = 0, \quad c_1 = 0 \qquad on \ \ y = 1 \end{aligned}\right\} \tag{26}$$

where prime denote differential with respect to y.

The set of first order boundary value problem is further simplified by introducing stream function ψ_1 (x, y) defined as

$$u_1 = -\frac{\partial \psi_1(x,y)}{\partial y}, \quad v_1 = -\frac{\partial \psi_1(x,y)}{\partial x} \tag{27}$$

into equations (21)-(26) and eliminating the dimensionless pressure p_1, to obtain

$$\frac{\partial^4\psi_1}{\partial y^4} + \frac{\partial^4\psi_1}{\partial x^4} + 2\frac{\partial^4\psi_1}{\partial x^2\partial y^2} - u_0\frac{\partial^3\psi_1}{\partial x\partial y^2} - u_0\frac{\partial^3\psi_1}{\partial x^3} + \frac{\partial^2 u_0}{\partial y^2}\frac{\partial\psi_1}{\partial x} = G1\frac{\partial\theta_1}{\partial y} + G2\frac{\partial c_1}{\partial y} \tag{28}$$

$$p_r\left(u_0\frac{\partial\theta_1}{\partial x} + \frac{d\theta_0}{dy}\frac{\partial\psi_1}{\partial x}\right) = \omega\left(\frac{\partial^2\theta_1}{\partial x^2} + \frac{\partial^2\theta_1}{\partial y^2}\right) \tag{29}$$

$$S_c\left(u_0\frac{\partial c_1}{\partial x} + \frac{dc_0}{dy}\frac{\partial\psi_1}{\partial x}\right) = \frac{\partial^2\theta_1}{\partial x^2} + \frac{\partial^2\theta_1}{\partial y^2} - gc_1 \tag{30}$$

while the corresponding boundary conditions become

$$\left.\begin{aligned} &\frac{\partial \psi_1}{\partial y} = u_0^{'},\ \frac{\partial \psi_1}{\partial x} = 0, \theta_1 = -\theta_0^{'}, c_1 = -c_0^{'} \qquad on\ \ y = 0 \\ &\frac{\partial \psi_1}{\partial y} = 0\ ,\ \frac{\partial \psi_1}{\partial x} = 0,\ \theta_1 = 0, c_1 = 0 \qquad on\ \ y = 1 \end{aligned}\right\} \tag{31}$$

Equations (28)-(31) are simplified further by introducing another form of solution which is wavelike, due to the nature of the walls. Therefore, we assumed the following form of solution

$$\psi_1(x,y) = \in \ell^{i\lambda x}\psi(\lambda,y),\ \theta_1(x,y) = \in \ell^{i\lambda x}\phi(\lambda,y), c_1(x,y) = \in \ell^{i\lambda x}\varphi(\lambda,y) \tag{32}$$

Substituting (32) into (28)-(31), we have

$$\psi^{iv} = i\lambda(u_0\psi^{"} - \lambda^2 u_0\psi - u_0^{"}\psi) + \lambda^2(2\psi^{"} - \lambda^2\psi) + G1\phi^{'} + G2\varphi^{'} \tag{33}$$

$$\omega\phi^{"} = ip_r\lambda(u_0\phi + \theta_0^{'}\psi) + \omega\lambda^2\phi \tag{34}$$

$$\varphi^{"} = iS_c\lambda(u_0\varphi + c_0^{'}\psi) + (\lambda^2 + g)\varphi \tag{35}$$

with the boundary conditions

$$\left.\begin{aligned} &\psi^{'} = u_0^{'},\ \ \psi = 0, \theta_1 = -\theta_0^{'}, c_1 = -c_0^{'} \quad on\ \ y = 0 \\ &\psi^{'} = 0,\ \ \psi = 0,\ \ \theta_1 = 0,\ \ c_1 = 0 \qquad on\ \ y = 1 \end{aligned}\right\} \tag{36}$$

We solve the boundary value problems (33)-(36), by considering another perturbation scheme for small λ(or K<<1) of the form

$$\psi(\lambda,y) = \sum_{j=0}^{\infty}\lambda^j\psi_j,\ \ \phi(\lambda,y) = \sum_{j=0}^{\infty}\lambda^j\phi_j,\ \varphi(\lambda,y) = \sum_{j=0}^{\infty}\lambda^j\varphi_j\ \ (j = 0, 1, 2....) \tag{37}$$

Substituting equation (37) into equations (33)-(36) and retaining up to order λ^2, we obtained the following sets of differential equations and the corresponding boundary conditions

$$0(\lambda^0): \psi_0^{iv} = G1\phi_0^{'} + G2\varphi_0^{'},\quad \omega\phi_0^{"} = 0,\quad \varphi_0^{"} = g\varphi_0 \tag{38}$$

$$\left.\begin{aligned} &0(\lambda): \psi_1^{iv} = i(u_0\psi_0^{"} - u_0^{"}\psi_0) + G1\phi_1^{'} + G2\varphi_1, \\ &\omega\phi_1^{"} = ip_r(u_0\phi_0 + \theta_0^{'}\psi_0),\quad \varphi_1^{"} = iS_c(u_0\varphi_0 + c_0^{'}\psi_0) + g\varphi_1 \end{aligned}\right\} \tag{39}$$

$$\left.\begin{aligned} &0(\lambda^2):\ \psi_2^{iv} = i(u_0\psi_1^{"} - u_0^{"}\psi_1) + 2\psi_0^{"} + G1\phi_2^{'} + G2\varphi_2^{'} \\ &\omega\phi_2^{"} = ip_r(u_0\phi_1 + \theta_0^{'}\psi_1) + \omega\phi_0,\quad \varphi_2^{"} = iS_c(u_0\varphi_1 + c_0^{'}\psi_1) + \varphi_0 + g\varphi_2 \end{aligned}\right\} \tag{40}$$

with the corresponding boundary conditions

$$\left.\begin{aligned} &\psi_0^{'} = u_0^{'},\ \ \psi_0 = 0, \phi_0 = -\theta_0^{'}, \varphi_0 = -c_0^{'} \quad on\ \ y = 0 \\ &\psi_0^{'} = 0,\ \ \psi_0 = 0,\ \ \phi_0 = 0,\ \ \varphi_0 = 0 \qquad on\ \ y = 1 \end{aligned}\right\} \tag{41}$$

$$\left.\begin{aligned} &\psi_j^{'} = 0,\ \ \psi_j = 0, \phi_j = 0, \varphi_j = 0 \quad on\ \ y = 0 \\ &\psi_j^{'} = 0,\ \ \psi_j = 0,\ \ \phi_j = 0,\ \ \varphi_j = 0 \quad on\ \ y = 1 \end{aligned}\right\} \forall j \geq 1 \tag{42}$$

The zeroth-order problems, made up of equations (17),(18) and (19) with boundary conditions (20) and the first order problems, made up of equations (38), (39) and (40) with the boundary conditions (41) and (42) are solved, using Adomian decomposition method (ADM) Chen and Lu [13] with MAPLE (14) software to obtain the expression for (u_0 , θ_0 and c_0), (u_1, v_1, θ_1 and c_1) and (u, θ and c) as the zeroth-order, first-order and total solutions, respectively.

The zeroth-order solutions are

$$\begin{aligned} u_0 = -\frac{1}{24\omega(6+g)}(&y(-48G1\omega - 8G1\omega g - 6G1\alpha - G1\alpha g - 24G1m1\omega - 4G1m1\omega g - 24G2\omega m2 \\ &- 48G2\omega - 6G1\alpha y^3 - G1\alpha y^3 g + 24y^2 G1m1\omega + 4y^2 G1m1\omega g - 24y^2 G1\omega - 4y^2 G1\omega g + \\ &12y^2 G1\alpha + 2y^2 G1\alpha g + 24y^2 G2\omega m2 - 24y^2 G2\omega - 12y^2 G2\omega g + 72y\omega G1g + 72y\omega G2 \\ &+ 12y\omega G2g\ )) \end{aligned} \tag{43}$$

$$\theta_0 = \frac{1}{2\omega}(2\omega + 2ym1\omega - 2y\omega + y\alpha - \alpha y^2) \tag{44}$$

$$c_0 = \frac{1}{2(6+g)}(-12 - 2g - 12ym2 + 12y + 6yg - 2gy^3 m2 + 2gy^3 + g^2 y^3 - 6gy^2 - g^2 y^2) \tag{45}$$

The first-order solutions are

$$\left.\begin{aligned} u_1 &= -\in[\psi_r' \cos\lambda x - \psi_i' \sin\lambda x], \quad v_1 = -\lambda \in[\psi_r' \cos\lambda x + \psi_i' \sin\lambda x] \\ \theta_1 &= \in[\phi_r' \cos\lambda x - \phi_i' \sin\lambda x], \qquad c_1 = \in[\varphi_r' \cos\lambda x - \varphi_i' \sin\lambda x] \end{aligned}\right\} \quad (46)$$

where the subscripts r and i denotes respectively, the real and imaginary part of the three functions ψ, ϕ and φ andλx is taken to be $\pi/2$ following Fasogbon (2010). The expressions obtained for these three functions using ADM via MAPLE involved large output of which only the graphical results are presented.

For the total (u, θ, c), we have the following solutions

$$u = u_0 + u_1 \quad (47)$$

$$\theta = \theta_0 + \theta_1 \quad (48)$$

$$c = c_0 + c_1 \quad (49)$$

Pressure drop

The fluid pressure at any point (x, y) is obtained from equations (8) and (9) as

$$p(x,y) = \int dp(x,y) = \int \left(\frac{\partial p}{\partial x}dx + \frac{\partial p}{\partial y}dy\right) \quad (50)$$

Using equations (16), (27), (32) and (37), on equation (50), we obtained to $O(\lambda^2)$

$$\left.\begin{aligned} &p(x,y) - C = (u_0'' + G1\theta_0 + G2c_0)x + \mathrm{Re}\,al[u_0\psi_0' - u_0'\psi_0 + \lambda(u_0\psi_1' - u_0'\psi_1) + \\ &\lambda^2\left(u_0\psi_2' - u_0'\psi_2 + \int u_0\psi_0 dy\right) + i\lambda\{-\psi_0' + \int \psi_0'' dy + \psi_2''' - G1\phi_2 - G2\varphi_2 + \lambda(-\psi_1' + \int \psi_1'' dy)\} \\ &+ i\{\psi_1''' - G1\phi_1 - G2\varphi_1 + \lambda^{-1}(\psi_0''' - G1\phi_0 - G2\varphi_0)\}] \in \ell^{i\lambda x} \end{aligned}\right\} \quad (51)$$

Where: C is an arbitrary constant.

Equation (51) can be written as Ω=p(x,y)-p(x,1) Fasogbon (2010), where Ω is the pressure drop which shows the differences between the pressure at any point y in the flow field with x being constant. The pressure drop Ω[0] and Ω[p] is at λx=0 or 2π and λx=π/2, respectively.

Skin friction (S_f), Nusselt number (N_U) and Sherwood number (S_h)

Using expressions (16), (27), (32) and (37) on equation (15), we have

$$S_f^0(0) = u_0'(0) \ \text{and} \ S_f^0(1) = u_0'(1) \quad (52)$$

$$S_f^1(0) = -\in \lambda\ell^{i\lambda x}[\psi_0''(0) + \lambda^2\psi_2''(0) + \lambda^2\psi_0(0)] \quad (53)$$

and

$$S_f^1(1) = -\in \lambda\ell^{i\lambda x}[\psi_0''(1) + \lambda^2\psi_2''(1) + \lambda^2\psi_0(1)] \quad (54)$$

where $S_f^0(0)$, $S_f^0(1)$ *and* $S_f^1(0), S_f^1(1)$ are the zeroth and first order Skin frictions at the irregular wall (y=0) and flat wall (y=1), respectively.

$$N_u^0(0) = \theta_0'(0) \ \text{and} \ N_u^0(1) = \theta_0'(1) \quad (55)$$

$$N_u^1(0) = \in \ell^{i\lambda x}[\phi_0'(0) + \lambda^2\phi_2'(0)] \quad (56)$$

and

$$N_u^1(1) = \in \ell^{i\lambda x}[\phi_0'(1) + \lambda^2\phi_2'(1)] \quad (57)$$

Such that $N_u^0(0)$, $N_u^0(1)$ and $N_u^1(0)$, $N_u^1(1)$ are the zeroth and first order Nusselt number at the irregular wall (y=0) and flat wall (y=1) respectively,

and

$$S_h^0(0) = c_0'(0) \ \text{and} \ S_h^0(1) = c_0'(1) \quad (58)$$

$$S_h^1(0) = \in \ell^{i\lambda x}[\varphi_0'(0) + \lambda^2\varphi_2'(0)] \quad (59)$$

and

$$S_h^1(1) = \in \ell^{i\lambda x}[\varphi_0'(1) + \lambda^2\varphi_2'(1)] \quad (60)$$

Such that $S_h^0(0)$, $S_h^0(1)$ and $S_h^1(0)$, $S_h^1(1)$ are the zeroth and first order Sherwood number at the irregular wall (y=0) and flat wall (y=1), respectively.

Discussion of the Zeroth-order, first-order and total results

The solutions for zeroth and first order problems subjected to appropriate boundary conditions were obtained. The expressions for u_0, θ_0 and c_0 (zeroth-order solutions), u_1,v_1, θ_1 and c_1 (first-order solutions) and those of u, v, θ and c (total solutions) have been evaluated numerically at various values of y for several sets of the parameters α, G1, G2, m1, m2, g, N, λ and ϵ. Following Vajravelu and Sastri (1978), Fasogbon (2010) and Loganathan *et al*. (2011), we took λ=0.001, 0.002, G1=G2=5, 10, m1=m2=-1,2, ϵ=0.25 and P_r=0.71. Other quantities (α, g, and N) are also varied with the flow system.

Discussion of the Zeroth-order results

Velocity profiles

In order to have a clear understanding of the physical problems studied in this section; physical meaningful numerical values were assigned to various parameters embedded in the problem. A comparison of the present results with those of the previous works (Vajravelu and Sastri, 1978; Fashogbon, 2006) are carried out by setting the said new parameters (i e N,m2,G2 and g) to zero. Excellent agreements were obtained (Figs. 2 and 3).

Figure 2 shows the zeroth-order velocity (u_0) profiles plotted against y when m1 =-1. It is clearly seen that in the presence of heat source $\alpha > 0$ with an increase in the free convection parameter G1, the velocity increases across the entire channel width (curves III and VI). When there is heat sink $\alpha < 0$ and the free convection parameter G1 increases, the velocity (u_0) profiles decrease across the entire width of the channel (curves I and IV). In the absence of heat generation or absorption ($\alpha = 0$), the fluid velocity increases in the first half of the channel width y = 0.5 and then decreases with an increase in the free convection parameter G1 (curves II and V). It is also discovered that when the heat source parameter increases with constant free convection parameter G1, the velocity u_0 increases considerably (curves I, II, III) and (curves IV,V,VI).

The velocity u_0 profiles when m1 = 2 is presented in Fig. 3. It is observed that the fluid velocity u_0 profiles increase generally as the free convection parameter G1 increases for all the values of heat generation parameter (curves I and IV,II and V,III and VI). On fixing the free convection parameter G1 and increasing the heat source parameter, it is noticed that the velocity (u_0) profiles also increase across the entire channel width (curves I,II and III) and (curves IV,V and VI). These results from (Figs. 2 and 3) are exactly the same as those in Vajravelu and Sastri (1978) when the embedded parameters (N, g, G2 and m2) are zero and a different approach is used.

Figure 4 depicts the effect of chemical reaction parameter g on the fluid velocity when m1 = m2 = -1. It is noticed that when there is an increase in g with constant value of the free convection parameters G1 and G2, the velocity u_0 decreases across the entire width of the channel (curves I,II,III) and (curves IV,V,VI). When the free convection parameters G1 and G2 increase with a fixed chemical reaction parameter g, the velocity increases up to a particular point on the channel width and then decreases (curves I and IV,II and V,III and VI).

The effects of chemical reaction parameter g on the velocity u_0 profiles, when m1 = m2 = 2 is presented in Fig. 5. Results (except the one involving fixed chemical reaction parameter g) which are similar to those obtained from Figure 4 are observed. For constant values of g, while the free convection parameters G1 and G2 increase, the velocity (u_0) increases across the entire width of the channel.

Figure 6 reveals the effects of the radiation parameter N on the velocity u_0 profiles when m1 = m2 = -1. It is clearly seen that an increase in N for fixed free convection parameters G1 and G2, leads to a decrease in velocity u_0 profiles across the channel width (curves I,II,III) and (curves IV,V,VI). An increase in each of G1 and G2 with a fixed radiation parameter N, leads to an increase in velocity u_0 profiles to a particular point on the width of the channel and then a decrease (curves I and IV,II and V,III and VI).

When m1 = m2 = 2, Fig. 7 describes the effect of radiation parameter N on the velocity u_0 profiles. It is noticed that when the free convection parameters G1 and G2 are fixed, the velocity u_0 profiles remain the same with an increase in radiation parameter N when G1 = G2 = 5 (curves I,II,III) and a decrease is observed when G1 = G2 = 10 (curves IV,V,VI). An increase in free convection parameters G1 and G2 with constant radiation parameter N, leads to an increase in the velocity u_0 profiles (curves I and IV,II and V,III and VI).

Temperature profiles

The discussion of zeroth-order temperature (θ_0) profiles is started by carrying out, a comparison of the present and previous results when all the embedded parameters in the problem are set to zero. Figure 8 presents the results of variation of the zeroth-order temperature with y when the new parameter (i.e N) is zero. It is clearly seen that when m1 = -1, the temperature (θ_0) profile increases with an increase in heat source parameter (curves I,II,III and IV,V,VI). It is also observed that in the absence of heat sink/source ($\alpha = 0$), the temperature (θ_0) profile is a linearly decreasing function of y while in the presence of heat sink or source, it is parabolic in nature. When m1 = 2, the temperature (θ_0) profile behaved in the opposite way for all values of heat parameter. It is found that these observations tally with the corresponding ones in Vajravelu and Sastri (1978).

Figure 9 shows the effects of radiation on the temperature θ_0 profiles. It is realized that an increase in the radiation parameter N with constant temperature ratio m1, the temperature (θ_0) profiles decrease across the entire channel width (curves I, II,III) and (curves IV,V,VI).

Concentration profiles

It is noticed from Fig. 10, that with an increase in the chemical reaction parameter g, when the concentration ratio parameter m2 =-1, the concentration (c_0) profiles remain almost the same on the width of the channel up to y = 0.30 followed by a slight increase (curves I, II and III). However, when m2 = 2, a decrease in concentration c_0 profiles is observed for an increase in chemical reaction parameter g (curves IV,V and VI).

Skin friction profiles

Figures 32 – 35 illustrates the behaviour of the first -order Skin friction S(1) as a function of the heat source parameter at both wall of the channel. It is observed from Fig. 32 that with an increase in the heat source parameter $\alpha > 0$, the Skin friction S(1) increases when m1 = -1 and decreases when m1 = 1 at the irregular wall y = 0 (curves I and III) and (curves II and IV). At the flat wall the Skin friction S(1) is slightly parabolic in nature (curves V and VII) and (curves VI and VII). When there is an increase in the temperature ratio m1, with constant free convection parameter G1, It is observed that there is a decrease in Skin friction S(1) at the irregular wall y = 0 (curves I and II, III and IV) while reverse is the case at the flat wall y = 1 (curves V and VI,VII and VIII). With an increase in G1 for a fixed value of m1 = -1, an increase in the Skin friction S(1) is noticed (curves I and III) and for a fixed value of m1 = 1, a decrease is observed (curves II and IV) at the irregular wall y = 0. Reverse is the case at the flat wall y = 1 (curves V and VII) and (curves VI and VIII).

Figure 33 reveals the effect of the embedded parameters on the Skin friction S(1) at both walls of the channel. We observed that when the temperature and concentration ratios m1 and m2 are increased with fixed G1 and G2, the Skin friction S(1) decreases at the irregular wall y = 0 (curves I and II,III and IV) while an increase in the Skin friction S(1) is noticed at the flat wall y = 1 (curves V and VI, VII and VIII). For an increase in the free convection parameters G1 and G2 with fixed temperature and concentration ratios m1 = m2 =-1, the Skin friction S(1) increases (lines I and III), but when m1 = m2 = 1, a decrease up to point $\alpha = 3.5$ followed by an increase in Skin friction S(1) is observed at the irregular wall y = 0 (lines II and IV). Reverse is the case at the flat wall y = 1 (lines V and VII) and (lines VI and VIII).

The effect of the chemical reaction parameter g on the Skin friction S(1) at both walls of the channel is depicted in Fig. 34. We discovered that an increase in the chemical reaction parameter g with constant free convection parameters G1 and G2, leads to a decrease in the Skin friction S(1) at the irregular wall y = 0 (lines I and II,III and IV) while at the flat wall y = 1, there is no changes in the Skin friction S(1) when G1 = G2 = 5 (lines V and VI). However, an increase before a decrease is noticed when G1 = G2 = 10 (lines VII and VIII). For an increase in the free convection parameters G1 and G2 with

constant chemical reaction parameter g, the Skin friction S(1) increases at the irregular wall y = 0 (lines I and III, II and IV) while a decrease is observed at the flat wall y = 1 (lines V and VII,VI and VIII).

Figure 35 shows the effect of radiation parameter N on the Skin friction S(1) at both walls of the channel. It is realized that with an increase in the radiation parameter N, when the free convection parameters G1 and G2 are fixed, the Skin friction S(1) remains the same up to a particular value of α and then decreases at the irregular wall y = 0 (lines I and II,III and IV). At the flat wall y = 1 when G1 = G2 = 5, there is no changes in the Skin friction S(1) (lines V and VI), but when G1 = G2 = 10 , there is also no change up to a certain value of α after which there exists an increase (lines VII and VIII). An increase in the free convection parameters G1 and G2 with constant radiation parameter N, leads to an increase in the Skin friction S(1) at the irregular wall y = 0 (lines I and III, II and IV) while a decrease is observed at the flat wall y = 1 (lines V and VII, VI and VIII).

Nusselt number profiles

Figures 36 – 38 illustrate the behaviour of the Nusselt number $N_u(1)$ at both wall of the channel. Fig. 36 shows the Nusselt number profiles against heat source parameter. It is clearly seen that with an increase in the heat source parameter α, the profiles are parabolic in nature at both walls (y=0,1) (curves I,II,III and IV)and (curves V,VI,VII and VIII), respectively. When the temperature ratio m1 increases with constant free convection parameter G1, there is a decrease in the Nusselt number $N_u(1)$ at the irregular wall y = 0 and an increase at the flat wall y = 1(curves I and II,III and IV) and (curves V and VI, VII and VIII) respectively. When free convection parameter G1 increases with constant temperature ratio m1, the Nusselt number $N_u(1)$ decreases at y = 0 and increases at y = 1 (curves I and III, II and IV) and (curves V and VII, VI and VIII), respectively.

Figure 37 gives the effect of the chemical reaction parameters, on the Nusselt number $N_u(1)$ at both walls of the channel. For an increase in the chemical reaction parameter g and constant free convection parameters G1 and G2, it is found that the Nusselt number $N_u(1)$ slightly decreases at the irregular wall y = 0 (lines I and II,III and IV). On the flat wall y = 1, no changes in the Nusselt number $N_u(1)$ is observed when G1 = G2 = 5 (lines V and VI), but an increase is noticed when G1 = G2 = 10 (lines VII and VIII). An increase in the free convection parameters G1 and G2 with constant chemical reaction parameter g, leads to a decrease in the Nusselt number $N_u(1)$ at the irregular wall y = 0 (curves I and III, II and IV) while an increase in the Nusselt number $N_u(1)$ is observed at the flat wall y = 1 (lines V and VII, VI and VIII).

The effect of the radiation parameter N on the Nusselt number $N_u(1)$ at both walls of the channel is presented in Figure 38. It is clearly seen that with an increase in the radiation parameter N, when the free convection parameters G1 and G2 are fixed, the Nusselt number $N_u(1)$ decreases at the irregular wall y = 0 (lines I and II, III and IV) while an increase in the Nusselt number $N_u(1)$ is noticed at the flat wall y = 1 (lines V and VI,VII and VIII). The Nusselt number $N_u(1)$ decreases with an increase in the free convection parameters G1 and G2 for a fixed radiation parameter N at the irregular wall y = 0 (lines I and III,II and IV) while reverse is the case at the flat wall y = 1 (lines V and VII,VI and VIII).

Sherwoodnumber profiles

Figures 39 – 41 illustrate the behaviour of the Sherwood number $S_h(1)$ at both walls of the channel. Fig. 39 shows that with an increase in the temperature and concentration ratios m1 and m2, respectively; for fixed values of G1 and G2, the Sherwood number $S_h(1)$ increases at the irregular wall y = 0 (lines I and II,III and IV). While reverse is the case at the flat wall y = 1 (lines V and VI,VII and VIII). An increase in the free convection parameters G1 and G2 with fixed values of m1 and m2, leads to a decrease in the Sherwood number $S_h(1)$ when m1 = m2 = -1(lines I and III) while an increase is observed when m1 = m2 = 1 (lines II and VII) at the irregular wall y = 0. Sherwood number $S_h(1)$ behaves in the opposite way in the case of flat wall y = 0 (lines V and VII) and (lines VI and VIII).

Figure 40 presents the effect of the chemical reaction g on the Sherwood number $S_h(1)$ at both walls of the channel. It is realized that with an increase in g when the free convection parameters G1 and G2 are constant, the Sherwood number $S_h(1)$ increases at the irregular wall y = 0 (lines I and II, III and IV). Correspondingly, a decrease in Sherwood number $S_h(1)$ is observed at the flat wall y = 1 (lines V and VI, VII and VIII). An increase in the free convection parameters G1 and G2 with a fixed chemical reaction parameter g, leads to a decrease in the Sherwood number $S_h(1)$ at the irregular wall y = 0 (lines I and III, II and IV), while an increase in the Sherwood number $S_h(1)$ is observed at the flat wall y = 1 (lines V and VII,VI and VIII).

The effect of radiation parameter N on the Sherwood number $S_h(1)$ on both walls of the channel is revealed in Figure 41. It is clearly seen that with an increase in the radiation parameter N for fixed free confection parameters G1 and G2, there is no change in the Sherwood number $S_h(1)$ when G1 = G2 = 5 (lines I and II), but an increase before a decrease is observed when G1 = G2 = 10 (lines III and IV) at the irregular wall y = 0 . However, at the flat wall y = 1 and for either G1=G2=5 or G1=G2=10, a decrease in Sherwood number $S_h(1)$ up to α= 0 before an increase is observed (lines V and VI,VII and VIII). When there is an increase in the free convection parameters G1 and G2 with a fixed radiation parameter N, a decrease in Sherwood number $S_h(1)$ is observed at the irregular wall y = 0 (lines I and III,II and IV) while an increase in Sherwood number $S_h(1)$ is noticed at the flat wall y = 1 (lines V and VII, VI and VIII).

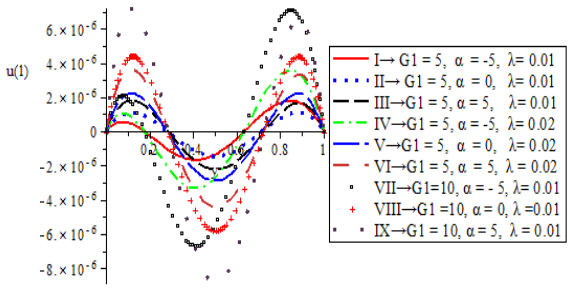

Fig.17 First-Order Velocity u(1) profile, m = -1, P =0.71, g=0,a=0,G2=0,m2=0,ε =0.25 and N=0

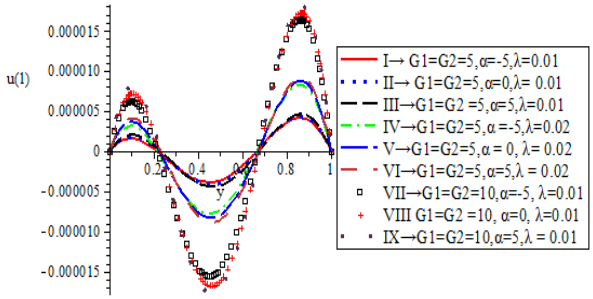

Fig. 18 First-Order Velocity u(1) profile, m = -1, P =0.71, g=4,a=0.60,m2=-1,ε =0.25 and N=5

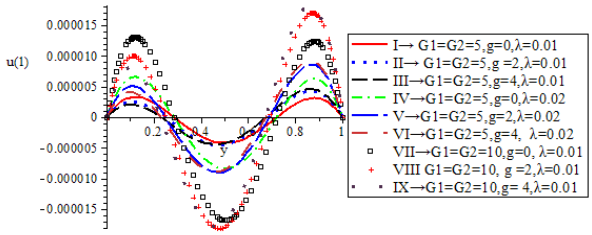

Fig. 19 First-Order Velocity u(1) profile, m =m2= -1, P =0.71, α=5,a=0.60,ε =0.25 and N=5

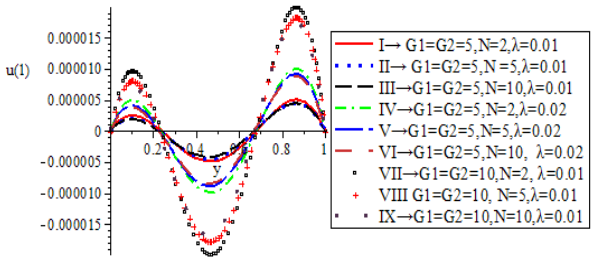

Fig. 20 First-Order Velocity u(1) profile, m =m2= -1, P =0.71, α=5,a=0.60,ε =0.25 and g=4

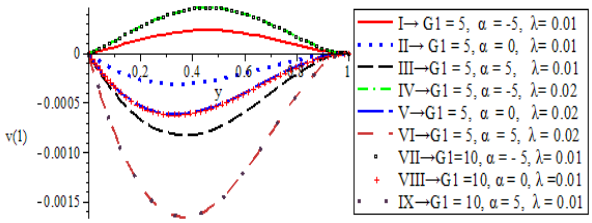

Fig 21 First-Order Velocity v (1) profile, m = -1, P =0.71, g=0,a=0,G2=0,m2=0,ε =0.25 and N=0

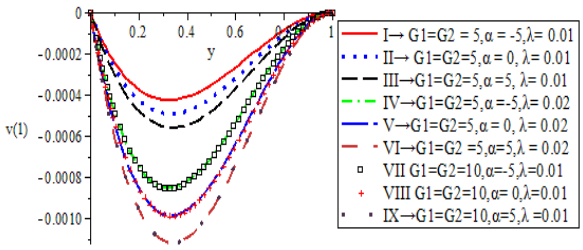

Fig. 22 First-Order Velocity v (1) profile, m1 =m2= -1, P =0.71, g=4,a=0.60,ε =0.25 and N=5

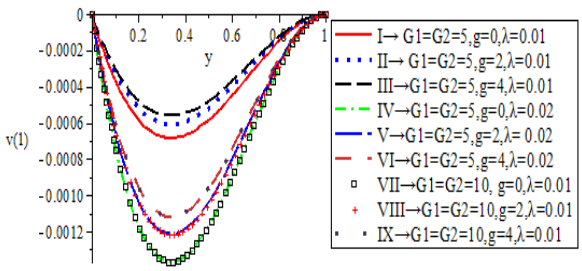

Fig. 23 First-Order Velocity v (1) profile, m1 =m2= -1, P =0.71, α =5,a=0.60,ε =0.25 and N=5

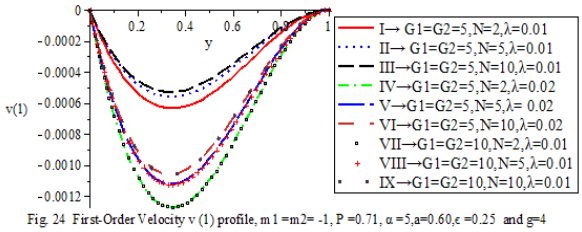

Fig. 24 First-Order Velocity v (1) profile, m1 =m2= -1, P =0.71, α =5,a=0.60,ε =0.25 and g=4

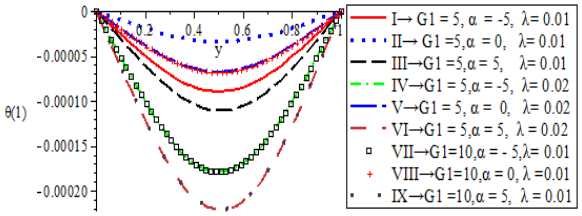

Fig. 25 First-Order temperature θ (1) profile, m1 = -1, P =0.71, g=0,G2=0,m2=0,ε =0.25 and N=0

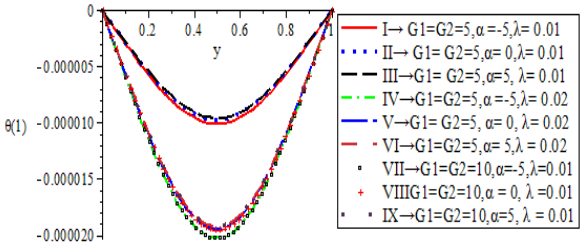

Fig. 26 First-Order temperature θ (1) profile, m1 = -1, P =0.71, g=4,m2=-1,ε =0.25 and N=5

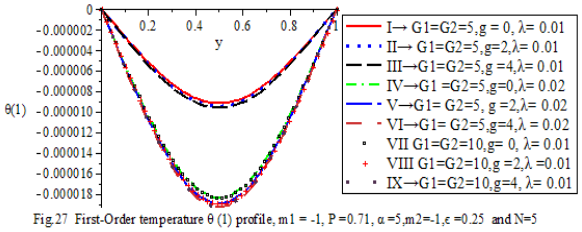

Fig.27 First-Order temperature θ (1) profile, m1 = -1, P =0.71, α =5,m2=-1,ε =0.25 and N=5

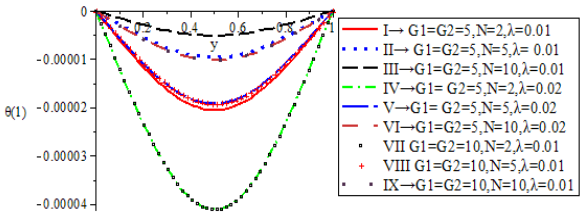

Fig. 28 First-Order temperature θ (1) profile, m1 = -1, P =0.71, α =5,m2=-1,ε =0.25 and g=4

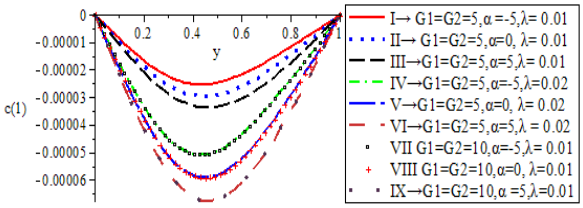

Fig. 29 First-Order Concentration c (1) profile, m1=m2=-1, a =0.60,g=4,ε =0.25 and N=5

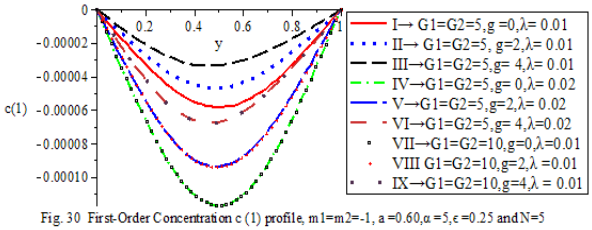

Fig. 30 First-Order Concentration c (1) profile, m1=m2=-1, a =0.60,α =5,ε =0.25 and N=5

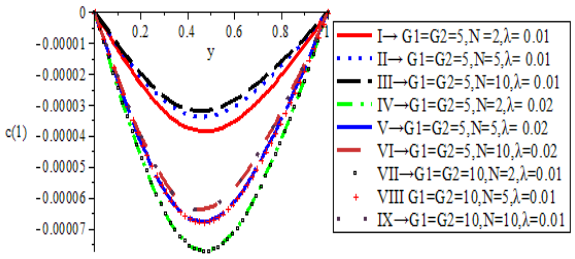

Fig. 31 First-Order Concentration c (1) profile, m1=m2=-1, a =0.60,α =5,ϵ =0.25 and g=4

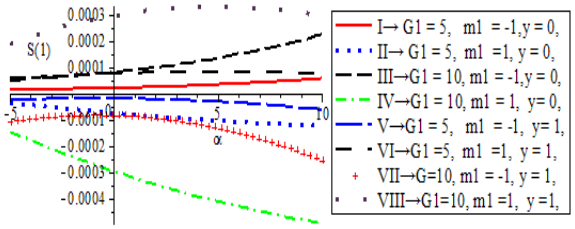

Fig.32 First-Order Skin Friction S (1) at y=0 and y=1,g=0,ϵ =0.25, p=0.71,m2=0, λ=0.01 and N=0

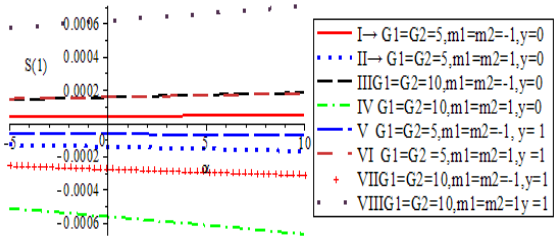

Fig. 33 First-Order Skin Friction S (1) at y=0 and y=1,g=4,ϵ =0.25,p=0.71, a=0.60, λ=0.01and N=5

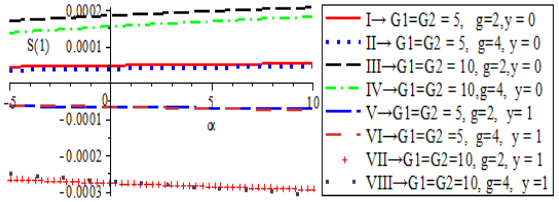

Fig. 34 First-Order Skin Friction S (1) at y=0 and y=1 ,m1=m2=-1,ϵ =0.25,p=0.71,a=0.60,λ= 0.01andN=5

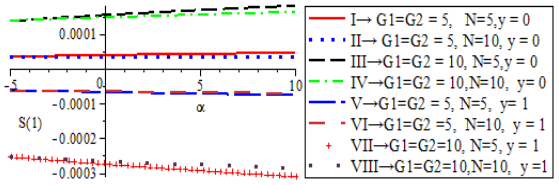

Fig. 35 First-Order Skin Friction S (1) at y=0 and y=1m1=m2=-1,ϵ =0.25,p=0.71,a=0.60,λ= 0.01andg=4

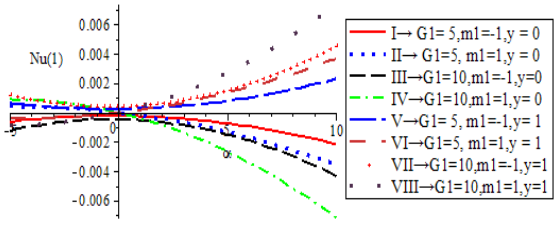

Fig. 36 First Order Nusselt Number Nu(1) m2=0,G2=0,N=0 ϵ=0.25,p=0.71,a=0.60,λ=0.01and g=0

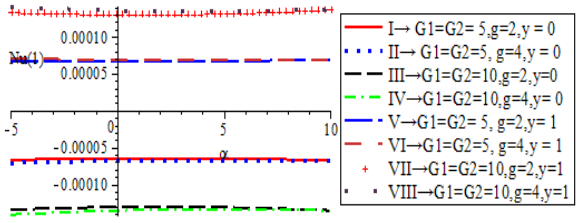

Fig. 37 First Order Nusselt Number Nu(1) at y=0 and y=1,N=5,ϵ =0.25,p=0.71,a=0.60,λ=0.01 and m1=m2=-1

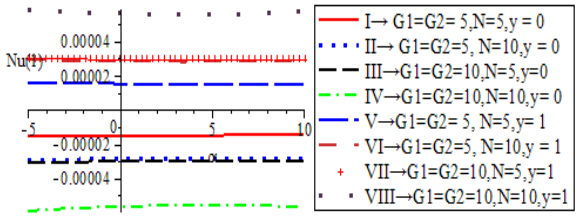

Fig. 38 First Order Nusselt Number Nu(1) at y=0 and y=1,g=4,ϵ =0.25,p=0.71,a=0.60λ= 0.01 and m1=m2=-1

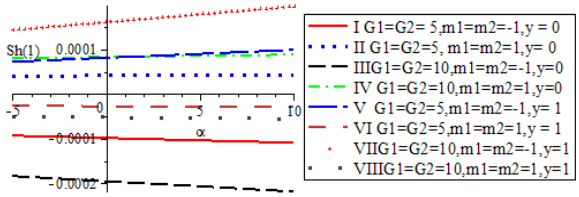

Fig. 39 First Order Sherwood Number Sh(1) g=4,ϵ =0.25,p=0.71,a=0.60,λ=0.01 and N=5

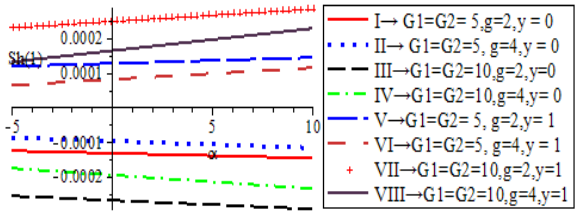

Fig. 40 First Order Sherwood Number Sh(1) N=5,ϵ =0.25,p=0.71,a=0.60,λ=0.01 and m1=m2=-1

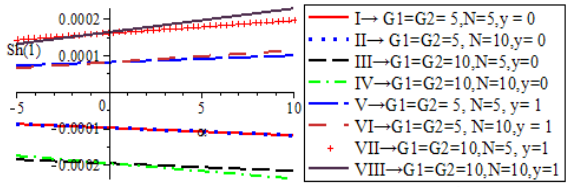

Fig. 41 First Order Sherwood Number Sh(1) g=4,ϵ =0.25,p=0.71,a=0.60,λ=0.01 and m1=m2=-1

Discussion of the total results

Figures 42 – 49 describe the total velocity (u) profiles along the length of the channel when the wall temperature ratio m1 and concentration ratio m2 are -1 and 2 respectively, for prandtl number p = 0.71. In particular, Figures 42 and 43 show the behaviour of the total velocity (u) profiles along the channel's length when the embedded parameters are zero. It is observed from Figure 42 that an increase in the heat source parameter with constant free convection parameter G1 and frequency parameter λ , leads to an increase in the total velocity profiles across the entire channel width (curves I,II,III), (curves IV,V,VI) and (curves VII,VIII,IX). The total fluid velocity(u) profiles do not vary with an increase in the frequency parameter λ when the free convection parameter G1 and heat source parameter α are kept constant (curves I and IV,II and V,III and VI). A decrease in the total fluid velocity

(u) profiles is observed for an increase in the free convection parameter G1 when the heat source parameter $\alpha < 0$ (curves I and VII).However, when $\alpha = 0$ an increase in the total velocity (u) profile up to a point y = 5 followed by a decrease is noticed (curves II and VIII), while an increase in velocity (u) is observed for $\alpha > 0$ (curves III and IX).

Figure 43 shows the behaviour of the total fluid velocity (u) profiles when m1 = 2. Apart from the case for which an increase in G1 with constant frequency parameter and heat source parameter , leads to an increase in the total velocity (u) profiles (curves I and VII,II and VIII,III and IX), the total velocity (u) profiles, in general, appear the same as we have in Fig. 42. When m1 = m2 =-1, Figure 44 depicts the effect of the embedded parameters on the total fluid velocity (u) profiles. It is realized that with an increase in the heat source parameter when free convection parameters G1, G2 and frequency parameter λ are kept constant, there is an increase in the total velocity (u)profiles. (curves I,II,III), (curves IV,V,VI) and (curves VII,VIII,IX). There is no changes in total velocity (u)profiles with an increase in the frequency parameter , when the heat source parameter and free convection parameters G1 and G2 are constant (curves I and IV,II and V,III and VI). Furthermore, an increase in the total fluid velocity(u) profiles up to some points on the width of the channel before a decrease is observed when there is an increase in the free convection parameters G1 and G2 with constant heat source parameter and frequency parameter (curves I and VII, II and VIII, III and IX).

Figure 45 reveals the behaviour of the embedded parameters on the total velocity (u) profiles when m1 = m2 = 2. It is noticed that an increase in the heat source parameter with constant free convection parameters G1, G2 and frequency parameter λ, leads to an increase in the total velocity (u)profiles (curves I,II,III), (curves IV,V,VI) and (curves VII,VIII IX). No changes in the total fluid velocity (u) profiles with an increase in the frequency parameter when heat source parameter and free convection parameters G1 and G2 are constant (curves I and IV,II and V,III and VI). However, an increase in the total velocity (u)profiles is noticed with an increase in the free convection parameters G1 and G2 when the heat source parameter and the frequency parameter are constant (curves I and VII, II and VIII,III and IX). When m1 = m2 =-1, Fig. 46 presents the effect of the chemical reaction parameter g on the fluid velocity (u) profiles. It is observed that with an increase in the chemical reaction parameter g when the free convection parameters G1, G2 and frequency parameter are constant, there is a decrease in the total fluid velocity (u) profiles (curves I,II,III), (curves IV,V,VI) and (curves VII,VIII,IX). An increase in the frequency parameter with constant free convection parameters G1,G2 and chemical reaction parameter g has no effect on the total fluid velocity (u)profiles (curves I and IV,II and V,III and VI). An increase in the total fluid velocity (u) profiles up to a particular point on the channel width before a decrease is observed when there is an increase in the free convection parameters G1 and G2 with constant chemical reaction parameter g and free frequency parameter (curves I and VII,II and VIII, III and IX).

Figure 47 shows the effect of chemical reaction parameter g on the total fluid velocity (u) profiles when m1 = m2 = 2. A decrease in the total velocity is observed with an increase in the chemical reaction parameter g when the free convection parameters G1, G2 and frequency parameter are constant (curves I,II,III), (curves IV,V,VI) and (curves VII,VIII,IX). No change in the total fluid velocity (u) is observed with an increase in the frequency parameter when chemical reaction parameter g and free convection parameters G1 and G2 are constant. However, with an increase in the free convection parameters G1 and G2 when chemical reaction parameter g and frequency parameter are kept constant, leads to an increase in the total fluid velocity (u) profiles (curves I and VII, II and VIII,III and IX).

The effect of radiation parameter N on the total fluid velocity (u) profiles when m1 = m2 =-1 is depicted in Fig. 48. It is noticed that the effect of radiation parameter N on the total fluid velocity is exactly the same as that of chemical reaction g (Fig. 46). When m1 = m2 = 2, Fig. 49 presents the effect of radiation parameter N on the total velocity (u) profiles. It is also noticed that the total fluid velocity (u) profiles behave the same way as when only the effect of chemical reaction g on it is being considered (Fig. 47).

Figures 50 – 55 present the behaviour of the total fluid temperature profiles. It is discovered from Figs. 50 and 51 which depict the variation of the total temperature for m1=-1 and 2 that with an increase in the heat source parameter and a fixed free convection parameter G1 and frequency parameter λ, there is an increase in the total temperature (θ) profiles (curves I,II,III), (curves IV,V,VI) and (curves VII,VIII,IX). When there is an increase in the frequency parameter λ (curves I and IV,II and V, III and VI) or free convection parameter G1 (curves I and VII,II and VIII, III and IX) with constant heat source parameter α, the temperature (θ) profiles remain unchanged throughout the entire channel width.

Figures 52 and 53 show the effect of the embedded parameters when m1 = m2 =-1 and m1 = m2 = 2, respectively. It is observed that the embedded parameters reduce the magnitude of the total fluid temperature (θ) profiles, while the behaviour of the total temperature (θ) still remain the same as we have in Figures (50 and 51).

Figures 54 and 55 reveal the effect of the radiation parameter N on the total temperature (θ) profiles when m1 = m2 =-1 and m1 = m2 = 2, respectively. It is noticed that an increase in the radiation parameter N with a fixed free convection parameters G1, G2 and frequency parameter λ, leads to a decrease in the total fluid temperature (θ) profiles (curves I,II,III), (curves IV,V,VI) and (curves VII,VIII,IX). Changes in the frequency parameter has no effect on the total fluid temperature (θ) profiles when the free convection parameters are constant (curves I and IV, II and V,III and VI). The same behaviour of the total fluid temperature is observed when the frequency parameter is constant with an increase in the free convection parameters G1 and G2 (curves I and VII,II and VIII,III and IX).

When m1 = m2 =-1, Fig. 56 presents the effect of the chemical reaction parameter g on the total fluid concentration (c) profiles. It is realized that with an increase in the chemical reaction parameter g and fixed values of G1, G2 and , the total fluid concentration (c) profiles remain the same up to the point y = 0.3 before an increase (curves I,II.III), (curves IV,V,VI) and (curves VII,VIII,IX). With an increase in free convection parameters G1 and G2 (curves I and VII,II and VIII, III and IX) or frequency parameter (curves I and IV,II and V, III and VI), the fluid concentration remains unchanged when g is constant.

Figure 57 shows the effect of the chemical reaction g on the fluid concentration (c) profiles when m1 = m2 = 2. A decrease in the total fluid concentration (c) is noticed with an increase in g when free convection parameters G1, G2 and frequency parameter are constant (curves I,II,III), (curves IV,V,VI) and (curves VII,VIII,IX). An increase in the free convection parameters G1, G2 (curves I and VII,II and VIII,III and IX) or frequency parameter (curves I and IV,II and V,III and VI), leads to no changes in the total fluid concentration (c) profiles.

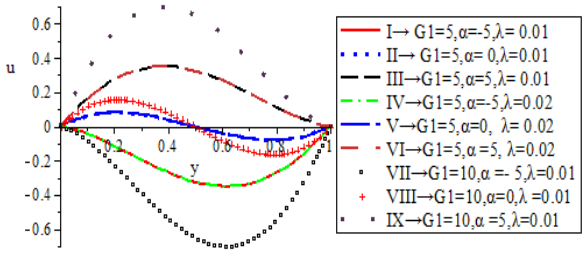

Fig. 42 Total Velocity(u) profile, m =-1, P =0.71,g=0,G2=0,a=0, m2=0 ,ϵ =0.25 and N=0

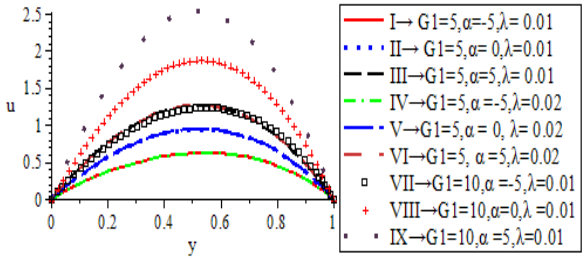

Fig. 43 Total Velocity(u) profile, m1 =2, P =0.71, g=0, G2=0, a=0, m2=0 , ϵ =0.25 and N=0

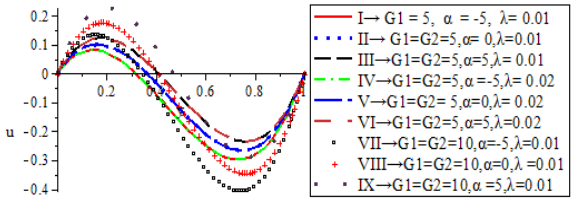

Fig. 44 Total Velocity(u) profile, m1 =-1, P =0.71,g=4,a=0.60, m2=-1,ϵ =0.25 and N=5

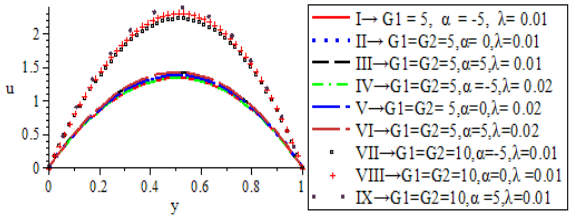

Fig.45Total Velocity(u) profile, m1 =2, P =0.71, g=4, a=0.60,m2=2, ϵ =0.25 and N=5

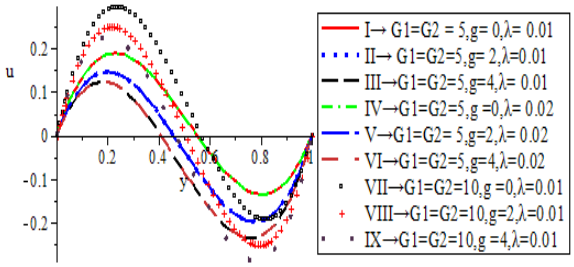

Fig. 46 Total Velocity(u) profile, m1 =-1, P =0.71,α=5,a=0.60,m2=-1,ϵ =0.25 and N=5

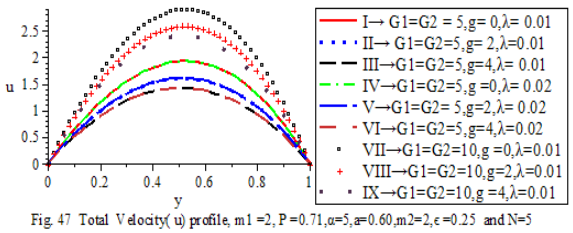

Fig. 47 Total Velocity(u) profile, m1 =2, P =0.71,α=5,a=0.60,m2=2,ϵ =0.25 and N=5

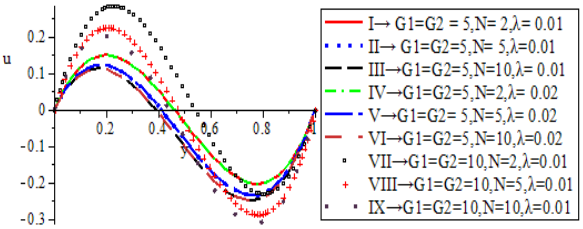

Fig. 48 Total Velocity(u) profile, m1 =-1, P =0.71,α=5,a=0.60,m2=-1,ϵ =0.25 and g=4

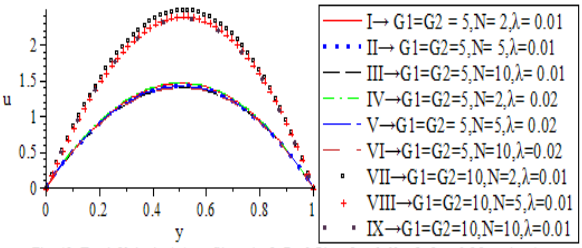

Fig. 49 Total Velocity(u) profile, m1 =2, P =0.71,α=5,a=0.60,m2=2,ϵ =0.25 and g=4

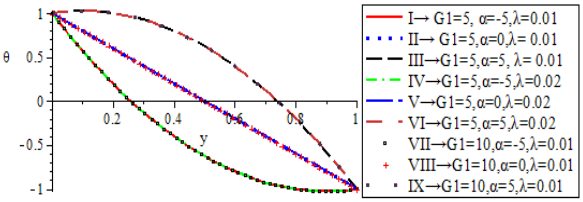

Fig. 50 Total temperature (θ)profile, m1 = -1, P =0.71, N =0,m2=0,ϵ =0.25 and g=0

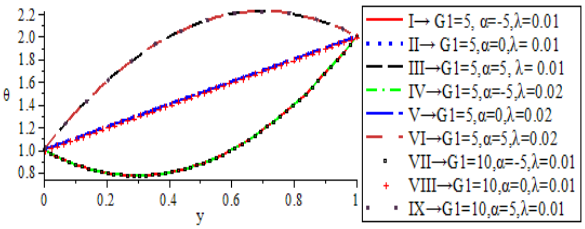

Fig. 51 Total temperature (θ)profile, m1 = 2, P =0.71, N =0,m2=0,ϵ =0.25 and g=0

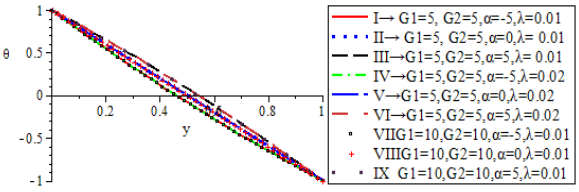

Fig. 52 Total temperature θ (1) profile, m1 = -1, P =0.71, N =5,m2=-1,ϵ =0.25 and g=4

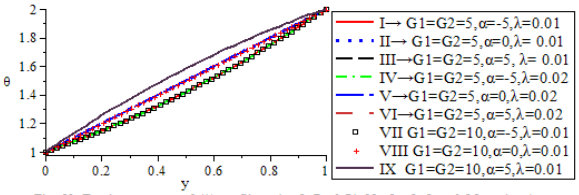

Fig. 53 Total temperature θ (1) profile, m1 = 2, P =0.71, N =5,m2=2,ϵ =0.25 and g=4

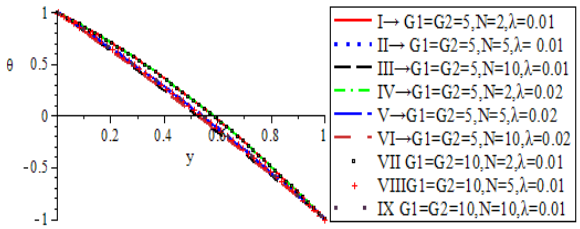

Fig. 54 Total temperature θ(1) profile, m1 = -1, P =0.71, g =4,m2=-1,ε =0.25 and α=5

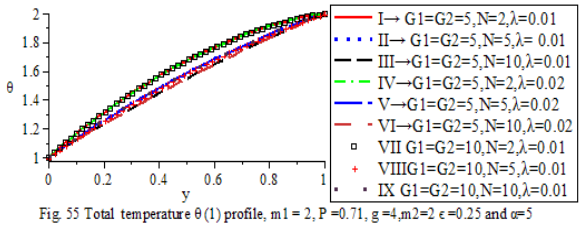

Fig. 55 Total temperature θ(1) profile, m1 = 2, P =0.71, g =4,m2=2 ε =0.25 and α=5

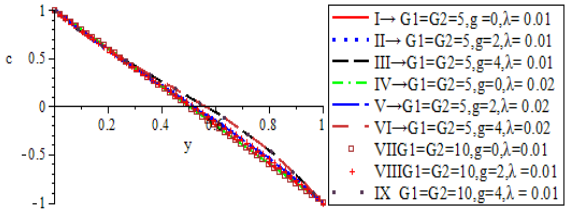

Fig. 56 Total Concentration c profile, m1=-1,m2=-1, a =0.60,ε =0.25 and N =5

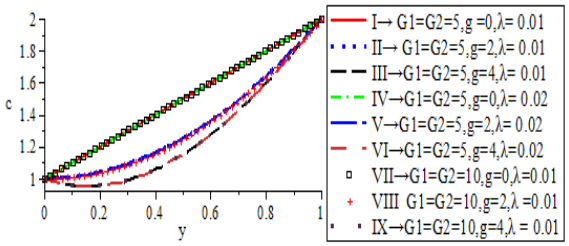

Fig. 57 Total Concentration c profile, m1=m2=2, a =0.60,ε =0.25 and N =5

Discussion of the pressure drops Ω[0] and Ω[P] results

The pressure drops Ω[0] at λx = 0 or 2π and Ω[p] at λx =π/2 are plotted against y in Figures 58-65 for m1=m2=-1. Figs. 58 and 59 illustrate the effect of the heat source parameter on the pressure drop Ω[0] and Ω[p], respectively. It is observed from Fig. 58 that an increase in the heat source parameter α, leads to a decrease in the pressure drop Ω[0]. While an increase in the pressure drop Ω[p] is noticed in Fig. 59 for an increase in heat source parameter α.

Figures 60 and 61 depict the effect of radiation parameter N on the pressure drops Ω[0] and Ω[p], respectively. Fig. 60 shows that the pressure drop Ω[0] increases with an increase in the radiation parameter N, while in Fig. 61, a decrease in the pressure drop Ω[p] is noticed for an increase in the radiation parameter N. The effect of chemical reaction parameter g on the pressure drop Ω[0] and Ω[p] are illustrated in Figs. 62 and 63, respectively. It is realized from Fig. 62 that the pressure drop Ω[0] decreases with an increase in the chemical reaction parameter g. Fig. 63 shows an increase in the pressure drop Ω[p] up to y = 0.1 and then a decrease, when there is an increase in the chemical reaction parameter g.

Figures 64 and 65 present the influence of the free convection parameters G1 and G2 on the pressure drops Ω[0] and Ω[p], respectively. Fig. 64 shows a decrease in the pressure drop Ω[0] with an increase in G1 and G2. In Figure 65, an increase in the free convection parameters G1 and G2, leads to an increase in the pressure drop Ω[p].Figs. 66 – 73 present the behaviour of the pressure drops Ω[0] at λx = 0 or 2 and Ω[p] at λx =2/π , when m1=m2=2. The effect of heat source parameter on the pressure drops Ω[0] and Ω[p] are shown in Figs. 66 and 67, respectively. It is observed from the Figs. that the pressure drops Ω[0] and Ω[p] increase with an increase in the heat source parameter .

The effect of radiation parameter N on the pressure drops Ω[0] and Ω[p] is respectively depicted in Figs. 68 and 69. It is noticed from the Figures that an increase in the radiation parameter N, leads to a decrease in the pressure drop Ω[0] and Ω[p]. Figs. 70 and 71 illustrate the influence of the chemical reaction g on the pressure drops Ω[0] and Ω[p], respectively. It is observed from Fig. 70 that an increase in the chemical reaction parameter g, leads to an increase in the pressure drop Ω[0] up to the values of y = 0.1 and then, a decrease. Fig. 71 shows the pressure drop Ω[p] increases with an increase in the chemical reaction parameter g (lines I and II), while an increase followed by a decrease is noticed line II and curve III.

Figures 72 and 73 give the effect of the free convection parameters G1 and G2 on the pressure drops Ω[0] and Ω[p], respectively. It is noticed from Fig. 72 that the pressure drop Ω[0] increases with an increase in G1 and G2, while a decrease in the pressure drop Ω[p] is realized in Fig. 73, when there is an increase in the free convection parameters G1 and G2.

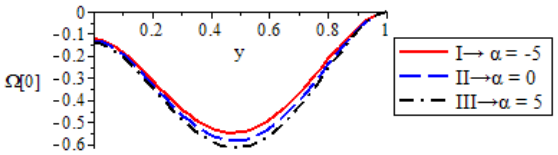

Fig. 58 Presure drop Ω[0] profile, m1=m2 =-1, G1=G2=5,N=5,λ=0.01,ε =0.25,p=0.71,a=0,60 and g= 4, λx=0 or 2π

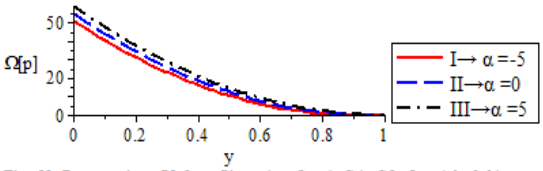

Fig. 59 Presure drop Ω[p] profile, m1=m2 =-1, G1=G2=5,g=4,λ=0.01,ε = 0.25,p=0.71,a=0,60 , N = 5, and λx=π/2

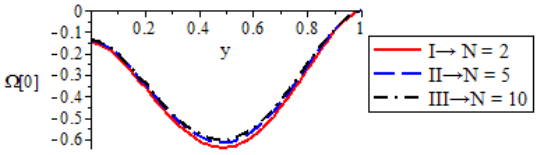

Fig. 60 Presure drop Ω[0] profile, m1=m2 =-1, G1=G2=5,α =5,λ=0.01,ε =0.25,p=0.71,a=0,60 and g= 4, λx=0 or 2π

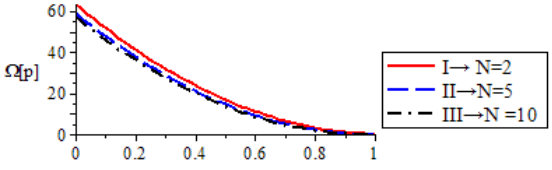

Fig. 61 Presure drop Ω[p] profile, m1=m2 =-1, G1=G2=5,g=4,λ=0.01,ε = 0.25,p=0.71,a=0,60 , α = 5, and λx=π/2

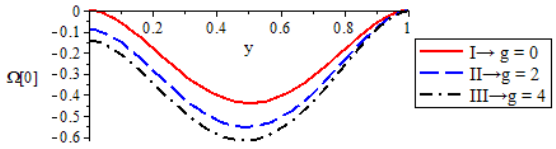

Fig. 62 Presure drop Ω[0] profile, m1=m2 =-1, G1=G2=5,N=5,λ=0.01,ϵ =0.25,p= 0.71,a=0,60 and α = 5,for λx=0 or 2π

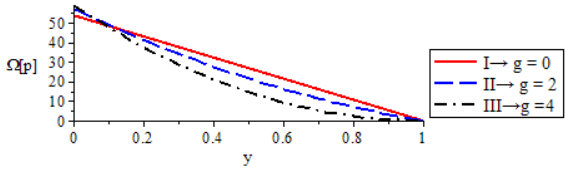

Fig. 63 Presure drop Ω[p] profile, m1=m2 =-1,G1=G2=5,N=5,λ=0.01,ϵ =0.25,p= 0.71,a=0,60 , α = 5, and λx=π/2

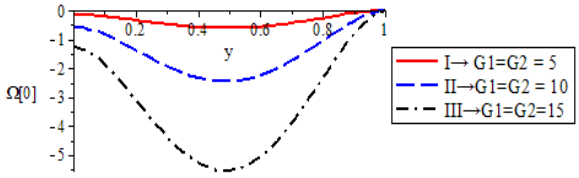

Fig. 64 Presure drop Ω[0] profile, m1=m2 =-1, g=4,N=5,λ=0.01,ϵ =0.25,p=0.71,a=0,60 and α = 5,for λx=0 or 2π

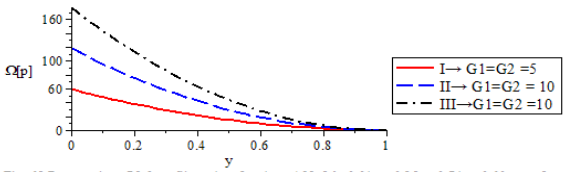

Fig. 65 Presure drop Ω[p] profile, m1=m2 =-1, g=4,N=5,λ=0.01,ϵ =0.25,p=0.71,a=0,60 , α = 5, and λx=π/2

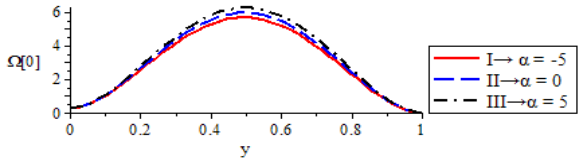

Fig. 66 Presure drop Ω[0] profile, m1=m2 =2, G1=G2=5,N=5,λ=0.01,ϵ =0.25,p= 0.71,a=0,60 and g= 4, λx=0 or 2π

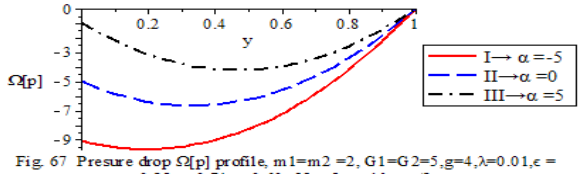

Fig. 67 Presure drop Ω[p] profile, m1=m2 =2, G1=G2=5,g=4,λ=0.01,ϵ = 0.25,p=0.71,a=0,60 , N = 5, and λx=π/2

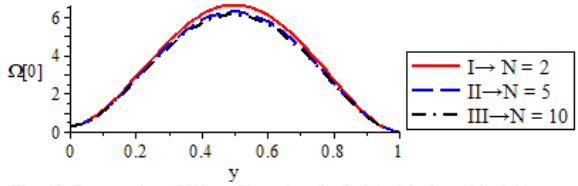

Fig. 68 Presure drop Ω[0] profile, m1=m2 =2, G1=G2=5,α =5,λ=0.01,ϵ = 0.25,p=0.71,a=0,60 ,g=4 and λx= π/2

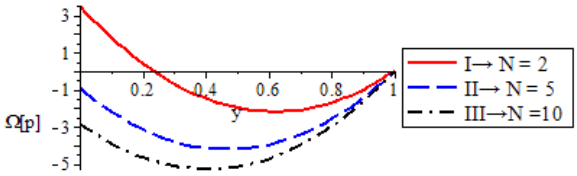

Fig. 69 Presure drop Ω[p] profile, m1=m2 =2, G1=G2=5,g=4,λ=0.01,ϵ = 0.25,p=0.71,a=0,60 , α = 5, and λx=π/2

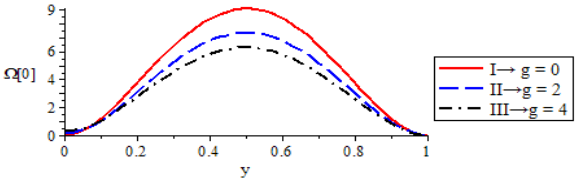

Fig. 70 Presure drop Ω[0] profile, m1=m2 =2, G1=G2=5,N=5,λ=0.01,ϵ =0.25,p= 0.71,a=0,60 , α = 5 and λx=0 or 2π

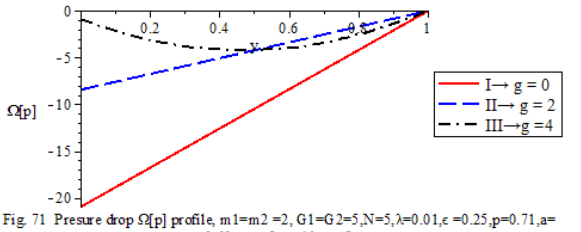

Fig. 71 Presure drop Ω[p] profile, m1=m2 =2, G1=G2=5,N=5,λ=0.01,ϵ =0.25,p=0.71,a= 0,60 , α = 5, and λx=π/2

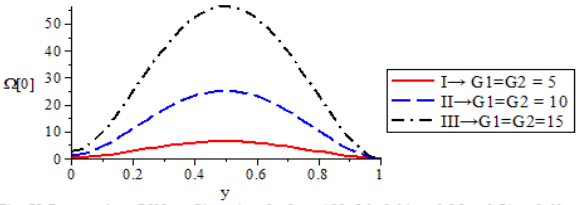

Fig. 72 Presure drop Ω[0] profile, m1=m2 =2, g=4,N=5,λ=0.01,ϵ =0.25,p=0.71,a=0,60 and α = 5 for λx=0 or 2π

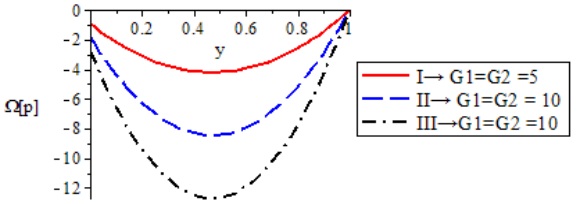

Fig. 73 Presure drop Ω[p] profile, m1=m2 =2, g=4,N=5,λ=0.01,ϵ =0.25,p= 0.71,a=0,60 , α = 5, and λx=π/2

Conclusions

An analysis of the effects of the thermal-radiation and chemically reacting on free convective heat and mass transfer flow of a viscous incompressible fluid within an irregular channel (made up of a long wavy wall at one end and a parallel flat wall at the other) is studied. The non-dimensional governing equations for the problems under consideration were expanded using perturbation method and solved, by applying Adomian decomposition method with MAPLE software. The expression for fluid variables (velocity, pressure, temperature and concentration) and some characteristics of heat and mass transfer (Skin friction, Nusselt number and Sherwood number) were obtained and evaluated numerically for various fluid parameters involved and the results presented graphically. The conclusions drawn are that the parameters g and N in the problems have played significant roles by influencing the behaviour of the fluid flow as follows;

(i) The velocity decreases with an increase in chemical reaction parameter g and radiation parameter N.
(ii)The temperature decreases with an increase in the radiation parameter N, while an increase in the temperature is observed with an increase in the chemical reaction parameter g.
(iii) The concentration increases with an increase in the chemical reaction parameter g.
(iv)The pressure drop increases with an increase in the radiation parameter N, while a decrease is observed when there is an increase in the chemical reaction parameter g.
(v)The Skin friction decreases with an increase in the chemical reaction parameter g at the irregular wall y = 0, while an increase is observed at the flat wall y = 1. With an increase in radiation parameter N, there is a decrease in skin friction up to $\alpha = 0$ and then an increase at the at wall y = 0, while reverse holds at the flat wall y = 1.

(vi) The Nusselt number decreases for $\alpha < 0$ while it increases for $\alpha > 0$ at the irregular wall y = 0, for an increase in g and N . At the flat wall y = 1, reverse holds for N, while it decreases for $\alpha < -2$ and then increases for $\alpha > -2$ when there is an increase in g.
(vii) The Sherwood number increases with an increase in g at the irregular wall y = 0, while a decrease in Sherwood number is observed at the flat wall y = 1. No change in Sherwood number is noticed at the irregular wall y = 0, with an increase in radiation parameter N. However, a decrease in Sherwood number up to $\alpha = 0$ before an increase is observed at the flat wall y = 1.

Nomenclature

C_0 -Species concentration at any point in the fluid
c - Dimensionless concentration
C_s -concentration susceptibility
c_w - Wall concentration
c_0 - Zeroth order concentration
c_1 - First-order concentration
c_p - Specific heat at constant pressure
G1 - Thermal Grashof number
G2 -Mass Grashof number
m1 - Temperature ratio
m2 - Concentration ratio
g_x - Acceleration due to gravity in x-direction
K_T - Fluid thermal diffusion ratio
k_1 - Chemical reaction parameter
k - Thermal conductivity
T ` -Dimensional temperature of the fluid
T_w - Wall temperature
T_1 - Temperature of the at wall
P` - Dimensional fluid pressure
p - Dimensionless fluid pressure
p_r - Prandtl number
Q - Heat generation/absorption
S_c - Schemit number
κ- wave number
ρ- Fluid density
β_c - Coefficient of concentration expansion
β_T - Volumetric coefficient of thermal expansion
α- Dimensionless heat source or sink parameter
U_0,V_0 -Velocity components along the (X,Y) axes
u,v - Dimensionless velocity
u_0- Dimensionless zeroth-order velocity
u_1,v_1–Dimensionless first-order velocity
X', Y` - Dimensional coordinate system
x,y -Dimensionless coordinate system
ϵ^*- Irregular wall amplitude
ϵ-Dimensionless amplitude
Ω- pressure drop
λ- Dimensionless wave length of the irregular wall
μ- Dynamic viscosity
ν- Fluid kinematic viscosity
θ- Dimensionless temperature of the fluid
θ_0 - Dimensionless zeroth-order temperature profiles
θ_1 - Dimensionless first-order temperature profiles
ψ_1 - stream function
g- Chemical reaction parameter
N - Radiation parameter
S_f - Dimensionless wall skin friction
N_u - Dimensionless Nusselt number
S_h -Dimensionless Sherwood number

References

Abubakar JU 2014. Natural convective flow and heat transfer in a viscous incompressible fluid with slip confined within spirally enhanced channel, Ph.D. thesis, University of Ilorin, Nigeria.

Adesanya SO 2013. Thermal stability analysis of reactive hydromagnetic third-grade fluid through a channel with convective cooling. *J. Nig. Math. Soc*., 32: 61-72.

Chen W & Lu Z 2004. An algorithm for adomian decomposition method. *Appl. Maths. & Computa*., 15:221-235.

Dada MS & Disu AB 2015. Heat transfer with radiation and temperature dependent heat source in MHD free convection flow in a porous medium between two vertical wavy walls.*J. Nig. Math. Soc*., http://dx.doi.org/10.1016/j.jnnms 2014.12.001.

Das UN & Ahmed N 1992. Free convective MHD flow and heat transfer in a viscous incompressible fluidconfined between a long vertical wavy wall and a parallel at wall. *Indian J. Pure Math*., 23(4): 295-304.

Davika B, SatyaNarayana PV & Venkataramana S 2013. Chemical reaction effects on MHD free convection flow in an irregular channel with porous medium.*Int. J. Math. Archive*, 4(4): 282-295.

Fasogbon PF 2006. Bouyancy driven flow in a rough channel. *J. Applic. Functional Differential Equation (JAFDE)*, 1(1): 45-58.

Fasogbon PF & Omolehin JO 2008. Radiation effect on natural convection in spirally enhanced channel. *leJEMTA* 3(1): 1-28. Fasogbon PF 2010. Analytical studies of heat and mass transfer by free convection in a two dimensional irregular channel. *Int. J. Appl. Math. & Mech.*, 6(4): 17-37.

Gbadeyan JA, Olanrewaju MA & Olanrewaju PO 2011. Boundary layer flow of a Nano-fluid past a stretching sheet with a convective boundary conditionin the presence of magnetic field and thermal radiation.*Australian J.Basic & Appl. Sci*., 5(9): 1322-1334.

Gbadeyan JA and Dada MS 2013. On the influence of radiation and heat transfer on anunsteady MHD non-Newtonian fluid flow with slip in a porous medium. *J.Maths. Res.*, 5(3): 40-50.

Hayat T, Abass Z, Pop I & Asghar S 2010. Effects of radiation and magnetic field on the mixed convection stagnation-point flow over a vertical stretching sheet in a porous medium. *Int. J. Heat & Mass Transfer*, 53: 466-474.

Kumar H 2011. Heat transfer with radiation and temperature dependent heat source in MHD free convection flow confined between two vertical wavy walls.*Int. J. Appl. Math. & Mech.*, 7(2): 77-103.

Loganathan P, Iranian D & Ganesan P 2011. Effect of chemical reaction on unsteady free convective and mass

transfer flow past a vertical plate with variable viscosity and thermal conductivity.*Eur. J. Scientific Res.*, 59(31): 403-416.

Olanrewaju PO & Gbadeyan JA 2011. Effect of Soret, Dufour, chemical reaction, thermal radiation and volumetric heat generation/absorption on mixed convection stagnation-point flow on an iso-thermal vertical plate in porous media.*Pacific J. Sci. & Techn.*, 12(20): 234-245.

Olanrewaju PO, Adeniyan A & Sanmi FA 2013. Soret and Dufour effects on hydromagnetic free convection flow with heat and mass transfer past a porous plate in the presence of chemical reaction and thermal radiation. *Far East J. Appl. Maths.*, 80(1): 41-66.

Oyekunle TL 2015. Thermal-diffusion, Diffusion-thermo and Radiation effects on chemically reacting magneto-hydrodynamics flow of heat and mass transfer within an irregular channel, Ph.D. thesis, University of Ilorin, Nigeria.

Rajasekhar NS, Prasad PMV & PrasadaRao DRV 2013. Effect of chemical reaction and radiation absorption on unsteady convective heat and mass transfer flow of a viscouselectrically conducting fluid in a vertical wavy channel with traveling thermal waves and Hall effects.*Int. J. Engr. Res. & Applic.*, 3(1): 1733-1747.

Sudershan Reddy G, Ramana Reddy GV & Jayarami Reddy K 2012. Radiation andchemical reaction effects on free convection MHD flow through a porous medium bounded by vertical surface.*Advances in Appl. Sci. Res.*, 3(3): 1603-1610.

Srihari K & Avinsh K 2014. Effect of radiation on unsteady MHD flow of a chemically reacting fluid past a hot vertical porous plate.*A Finite Difference Approach*, 5(1): 50-69.

Shateyi S, Motsa SS & Sibanda P 2010. The effect of thermal radiation, Hall currents, Soret and Dufour on MHD flow by mixed convection over a vertical surface in a porous media.*Mathematical Problems in Engineering*, Article ID 62747:20 pages.

Vajravelu K & Sastri KS 1978. Free convective heat transfer in a viscous incompressible fluid confined between a long vertical wavy wall and a parallel at wall. *J. Fluid Mech*., 86(2): 365-383.